CORROSION RESISTANCE OF STEEL REINFORCEMENTS EMBEDDED IN ALKALI ACTIVATED GROUND GRANULATED SiMn SLAG MORTARS

R. Navarro[1], E.G. Alcocel[2], I. Sánchez[1], P. Garcés[1], E. Zornoza[1]

1. *Dept. of Civil Engineering. University of Alicante (Spain)*
2. *Dept. of Architectonic Constructions. University of Alicante (Spain)*

ABSTRACT

The corrosion process of steel reinforcements embedded in alkali activated SiMn slag mortars was investigated. NaOH and waterglass were used as alkali activators of SiMn slag. The steel reinforced mortars were subjected to two aggressive environments: carbonation and chloride ingress. Carbonation progressed quicker for the binder activated with NaOH, decreasing the rate with the concentration. However, during the corrosion of the steels embedded in the mortars, both activators showed a similar behaviour. Mortars prepared with waterglass exhibited higher chloride migration coefficients, which decreased as the activator concentration increased. In a chloride contaminated ambient, steel embedded in mortars prepared with NaOH offered lower corrosion rate levels and it increased with the activator concentration.

Keywords: SiMn slag; alkali activation; corrosion; carbonation; chloride; steel

1. INTRODUCTION

In 1957 Glukhovsky proposed a hypothesis in which a close relationship was established between the alkalis and the cementing materials. This hypothesis has served as the basis for the development of a new class of cementitious materials called "alkaline cements" [1]. The alkali-activated materials (AAMs) are prepared with aluminosilicates that are attacked by alkaline activators [1,2]. The most used aluminosilicates are: ground granulated blast furnace slag [3,4], fly ash [5] and metakaolin [6]. In the side of activators, most of research has paid attention to caustic alkalis, silicates, carbonates and sulfates [7]. AAMs are classified into two kinds of gel systems: high-calcium and low-calcium systems. High-calcium system is dominated by calcium alumina silicate hydrate $CaO\text{-}Al_2O_3\text{-}SiO_2\text{-}H_2O$ (C-A-S-H) gels with tobermorite-like structure, such as alkali-activated slag. While in low-calcium system, also named “geopolymers”, are dominated by alkali aluminosilicate $Na_2O\text{-}Al_2O_3\text{-}SiO_2\text{-}H_2O$ (N-A-S-H) gels with pseudo-zeolitic structure, like alkali-activated fly ash [1,2,8].

In recent years there has been an exponential growth of research related to this type of alternative binders, and it is currently when they are acquiring true technological significance. The reason why they have gained recognition and interest after so many years of sporadic use is due to their potential contribution to the reduction of CO_2 emissions compared to those produced by Portland cement since the majority of alkaline activated materials are industrial by-products and, therefore, with low ecological footprint [2]. Different authors have shown the benefits in terms of lower energy consumption and environmental impact [9–12]. However, AAMs present some problems like the cost of raw materials and the unknown performance of long-term durability [13]. In particular, if AAMs are devoted to their use in structural applications, they need to offer steel corrosion protection as Portland cement-based concretes do. Therefore, two main aggressive environments have to be considered for a steel reinforced concrete in terms of resistance to corrosion: high concentrations of atmospheric CO_2 and chloride ingress from different sources (marine, de-icing salts, etc).

In terms of corrosion resistance, the predominant aqueous medium of the pore solution and the cover transport properties are the key factors. Any steel reinforced concrete needs a solution in the pores of pH high enough to passivate the embedded steel. Thus, given the high pH of alkaline activated systems which is usually higher than 13.5, and even 14.5 in some systems, passivation should be achieved directly. However, such a high pH levels also may induce the formation of non-stable passivating films on the steel surface [14]. Apart from this aspect, since there is no solid pH-regulating phase such as portlandite in the medium, the ability to maintain high

alkalinity relies in the prevention of acid substances (H^+ or CO_2) from entering and/or to avoid the washing of alkaline substances from the solution in the pores. Therefore, the porous structure (porosity and tortuosity) together with the chemical considerations of alkaline activated binders are determinant for durability performance [8]. Related to the refinement of the porous structure and with the adequate acquisition of mechanical strength, it is necessary to select suitable curing conditions to avoid microcracking and guarantee an adequate performance in service. These systems require a careful specification and control of curing that allows them to reach an adequate maturity before entering in service or being tested.

Many critical aspects related to durability such as carbonation, chloride penetration and attack by sulphates, are related to water absorption capacity and permeability, which in turn are influenced by multiple factors such as precursors, activators, maturity, aggregate-paste interface and test methods (especially the conditioning aspects by pre-drying that can cause the appearance of microcracks) [13,15].

Several authors have investigated the carbonation process of the AAS mortars under accelerated carbonation conditions [16–20], chloride penetration [21–23] and electrochemical behaviour of steel in alkali-activated slag mortars [24,25]. Their main conclusions established that the formation and stability of the passivating film depend on the nature and dosage of the binder, and the environmental conditions as well. In additions, it is pointed out that more research is needed on this specific topic.

Recently, it has been reported that some minority components of the slag, such as sulphide and manganese, may experience redox processes that could affect somehow to the corrosion of the steels embedded in alkali-activated slag mortars [26]. Those results showed highly negative corrosion potentials and high current density values in the presence of chloride. However, the surface of steel bars did not show evident corrosion signs. It was concluded that the presence of sulphide may reduce the redox potential of the pore solution, but it enabled the steel to remain in an apparent passive state. In addition, the high presence of MnO in the slag did not significantly affected the corrosion process. For these reasons, and considering that the SiMn slag used in the present research shows a high MnO content (about 12%), which is mainly dispersed in the vitreous phase, but also MnS is detected in XRD analysis, which could undergo additional oxidation, it is interesting to study the corrosion process of steels embedded in alkali-activated SiMn slag mortars.

In present study, the SiMn slag has been used as AAM. The chemical, mineralogical and pozzolanic characteristics of the SiMn waste allow its use as a substrate to obtain alkaline activated materials [27,28]. Previous studies have shown that it is possible to activate the ground SiMn residue with an efficient grinding process, using NaOH and waterglass as activators [27,28]. High enough mechanical performance was obtained, so it was concluded its possible use for both masonry and structural applications [27–29]. However, to completely enable the structural use, it is necessary to check the protection that it offers to steel reinforcements against the most classical corrosion processes.

The aim of this research is to evaluate the protection offered by mortars of alkali activated SiMn slag against the corrosion of steel reinforcements. To carry out this study, it was analysed whether the chemical environment generated by this binder with two different activators (sodium hydroxide and waterglass solutions) succeeds in the steel passivation process. After this, it has been investigated the corrosion resistance under two different aggressive processes: carbonation and chloride presence.

2. EXPERIMENTAL

2.1 Materials

SiMn slag was used as substrate for the binder preparation in this study. This slag was supplied by the Ferroatlántica plant placed at Boo-de-Guarnizo (Cantabria, Spain). The chemical composition of the slag is presented in Table 1. This SiMn slag is an acid slag with moderate

hydraulicity [30–32] as indicated by its basicity coefficient of 0.73 and its hydraulicity index of 0.85 [27].

Table 1. Chemical composition of the SiMn slag.

	SiO_2	CaO	MnO	Al_2O_3	MgO	Fe_2O_3	K_2O	Na_2O	SO_3	N.D.	L.O.I.
wt %	36.53	29.10	12.23	9.86	4.69	0.92	1.08	0.34	2.77	2.48	-1.25

The slag mineralogy was identified by X-ray diffractometer (PANalytical, model EMPYREAN) operated at 50 mA and 50 kV, using Mo$K_{\alpha 1}$ radiation. The scanning of diffraction angle (2θ) varied from 3° to 35° at a step size of 0.0113°/step for 5 hours. The vitreous phase content applying Rietveld method [33] was 96.0±1.5%. The slag selected in this work has a 33.80% of reactive silica according to the standard UNE 80225-2012 [34]. Regarding insoluble residue, the obtained result was a 3.35% following the standard UNE 196-2-2014 [35]. Therefore, as commented in other previous studies [27,29], the high content of silicon, calcium and aluminium oxides of this slag, together with its content of reactive silica and vitreous phase, make this material able to be alkali-activated. Negative LOI value could be associated to oxidation of S-rich species in the slag [17].

The size at which the granulated SiMn slag was supplied was not adequate for mortar mixing. Consequently, the dry slag was ground in a laboratory ball mill Nanneti model SPEEDY 1 for 25 minutes until it reached a fineness of 5512 cm^2/g. This result was obtained using the Blaine's air permeability method of the standard UNE EN 196-6:2010 [36]. According Wang et al. [32], the optimum range of slag fineness was 4500-6500 cm^2/g for acid slags. The particle size range of slag, determined by a laser diffraction equipment (Malvern Instruments, model Mastersizer 2000), was 0.32–113.58 µm, with a $D_{V,50}$= 9.2 µm and a $D_{4,3}$ = 15.2 µm. The density of this SiMn slag is 2.916 g/cm^3.

On the other hand, sodium hydroxide (NaOH) and waterglass (WG) prepared with a commercial sodium silicate (Na_2SiO_3, neutral solution QP, Panreac: SiO_2/Na_2O molar ratio of 3.28) and sodium hydroxide (technical grade, Panreac) were used as alkaline solutions to activate the SiMn slag. Two different types of activators (NaOH and WG) and three different activator concentrations have been used in this study: NaOH solution with a 3.0%, 3.5% and 4.0% of Na_2O; and WG solution with a 4.0%, 4.5% and 5.0% of Na_2O and SiO_2/Na_2O ratio=1.00. The solution/slag ratio was 0.37 for mortars prepared with NaOH, and 0.40 for those ones prepared with WG. These dosages were chosen from previous studies [29], which evaluated the influence of $\%Na_2O$, SiO_2/Na_2O ratio and activating solution/slag ratio on the following selected control parameters: workability, compressive strength at 7, 28 and 90 days of curing time, setting times and shrinkage at 50% of relative humidity.

Silica sand was used as aggregate to prepare the mortars. This aggregate was characterized by the determination of fineness modulus [37], water absorption and density [38]. The values obtained for each of these properties were: fineness modulus=3.8, water absorption=0.2% and density=2.5 g/cm^3.

2.2 *Sample preparation*

Mortars were prepared using an aggregate/slag ratio of 2/1. In a previous work [29], the mechanical performance and dimensional stability of mortars incorporating different types of aggregates with different aggregate/slag ratios were studied. The best flexural and compressive strength results were obtained for an aggregate/slag ratio of 2/1 when silica sand was used as aggregate. This is the reason why this relationship has been chosen to study the properties of carbonation and corrosion in the present work.

In this way, each mortar was prepared by the mixing of 675 g of ground granulated SiMn slag, 1350 g of silica sand and the calculated quantity of alkaline solutions. Samples were prepared in a mixer Controls Automix (model 65-L0006/A) according to the standard UNE EN 196-1 [39].

2.3 *Experimental procedure*

2.3.1 Accelerated carbonation rate test

To perform this test, 40 × 40 × 160 mm mortar specimens for each mix were fabricated. The samples were cured in a 100% relative humidity (RH) environment for 90 days at 20 ± 2°C. Such long curing time was selected in order to achieve a high extension of the activation process, so the changes in the specimens can be only originated by the aggressive environments (carbonation and chloride ingress). In addition, the shrinkage of the specimens is reduced and it is avoided the appearance of cracks that would alter the ingress kinetics of carbon dioxide, chloride and oxygen. Then, these samples were taken from the humid chamber and kept for three weeks under laboratory conditions (20 ± 2°C and 50 ± 5% RH). This period of stabilization allows the water stored inside the pores to evaporate and accelerates the carbonation process. After these three weeks, the samples were introduced into a carbonation chamber with an approximately 100% CO_2 atmosphere at 65 ± 5% RH for 50 days in order to ensure the complete carbonation of samples. During the carbonation test, carbonation depth was measured using the phenolphthalein test according to the standard UNE/112011:1994 [40]. In this test, the surface obtained after breaking the sample is sprayed with a phenolphthalein solution of 1% in water/ethanol 1:1. The colourless part corresponds to the carbonated area and the carbonation depth was obtained after measuring the thickness in the four sides of the cross section.
Additionally, other samples were subjected to the same carbonation process, but after 50 days of the carbonation process, they were mechanically tested by measuring the compressive and flexural strengths in a hydraulic press according to the standard EN 196-1 [39].

2.3.2 Corrosion rate test

The specimens for corrosion test were steel reinforced mortar cylinders with a diameter of 5 cm and a height of 10 cm. Each specimen contains three steel bars (Ø 6 mm). Figure 1 shows a scheme of the specimens used in this study. The exposed area of each steel bar has been 12.3 cm^2 and the resulting mortar cover is 7 mm. To limit the exposed surface area of each steel, an insulating tape was applied as it is shown in Figure 1.

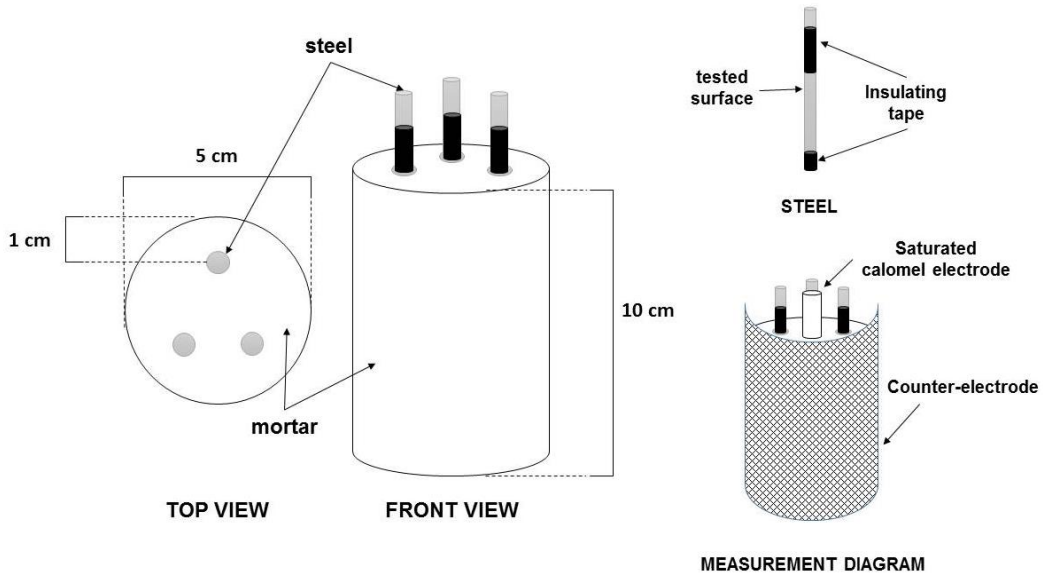

Figure 1. Specimens used in corrosion rate study.

For each type of mortar (two activators: NaOH and WG; three different concentrations for each activator), seven different environments were analysed:

- A control specimen was stored in the humid chamber during the curing and then in laboratory conditions.

- A specimen was subjected to an accelerated carbonation process in order to analyse the influence of this process on the corrosion of steel bars.
- A specimen partially submerged in simulating seawater (3.5% wt. of NaCl) in order to analyse the influence of external chlorides on the corrosion of steel bars.
- Four specimens were fabricated incorporating four different concentrations of NaCl (0.5, 1.0, 2.0 and 4.0% wt. of chloride by slag mass) in the activating solution during the mortar mixing in order to study the chloride content threshold needed for depassivating the steels embedded in the mortars.

As a result, seven specimens were fabricated from each system studied to evaluate the influence of each condition.

All the prepared specimens were cured in a 100% RH environment for 90 days at 20 ± 2°C. Then, they were stored under laboratory conditions (20 ± 2°C and 50± 5% RH) for three weeks. After this period, the control specimens and the specimens with different concentrations of internal chlorides were kept under the same conditions, that is, 20 ± 2°C and 50 ± 5% RH. On the other hand, the specimens designed to study the carbonation process were introduced into a carbonation chamber with a 100% CO_2 atmosphere at 65 ± 5% RH. Additionally, the specimens designed to analyse the influence of external chlorides were partially immersed in the simulating seawater.

During the corrosion tests, both corrosion potential (Ecorr) and corrosion rate (Icorr) were monitored periodically until the end of the test. All corrosion potentials are referred to a saturated calomel electrode (SCE). As counter-electrode, a stainless steel mesh was used. This mesh contacted the specimen through a wet cloth wrapped around the specimen. Corrosion rate measurements were based on the polarization resistance technique [41] using an Autolab potentiostat galvanostat (model PGSTAT30). The potential scan was made from −10 mV to +10 mV respect to the corrosion potential of each steel electrode. The scanning rate was 1.0 mV/s. Ecorr and Icorr values presented in this work refer to the mean values of three electrodes embedded in each specimen.

2.3.3 Chloride migration test

The migration test specimens were cylinders with a diameter of 10 cm and a height of 15 cm. After demoulding the mortars, they were cut obtaining cylinders 5 cm thick. The samples were cured a humid chamber in a 100% RH environment for 90 days at 20 ± 2°C. The forced chloride migration test was performed on water-saturated mortar samples, according to NT Build 492 [42] whose main result is the non-steady-state chloride migration coefficient (D_{NTB}). The chloride migration coefficient determined by this method is a measure of the resistance of the tested material to chloride penetration. For each mortar type (two activators: NaOH and WG; three different concentrations for each activator), four samples were tested.

2.3.4 Capillarity test

The test was carried out following the UNE EN 1015-18: 2003 standard [43]. Mortar specimens of 40 × 40 × 160 mm dimensions were fabricated for each of the dosages to be studied (two activators: NaOH and WG, three different concentrations for each activator). Samples were cured in a 100% RH environment for 90 days at 20 ± 2°C. After this curing period, the specimens were taken out, and each one was cut in two halves with the help of an electric disc cutter. Two halves of each dosage were obtained. The decision to cut the test pieces with electric cutter and not break them upon flexural stress, as indicated by the standard, was taken to get a flat face that facilitates the experimental assembly. The test pieces were dried in an oven at 60 ± 5°C until reaching a constant mass. The dried specimens were weighed (M_i). The specimens were placed on a tray with the broken faces of the prisms facing down, so that they do not touch the bottom of the tray and were immersed in water up to a height of 5 mm to 10 mm for the duration of the test. The tray was covered in order to avoid evaporation on the surface of the submerged samples. The specimens are removed after 10 min, 90 min and 24 hours. At those times, the

water on the surface is quickly removed with a damp cloth and weighed to obtain M_{10min}, M_{90min} and M_{24h}, respectively. Capillary absorption coefficient at 90 min (C_{90min}) and at 24 hours (C_{24h}) were be calculated according to the equations 1 and 2 shown in the standard [43].

Equation 1 $$C_{90min} = 0.1 \cdot (M_{90min} - M_{10min})$$

Equation 2 $$C_{24h} = 0.625 \cdot (M_{24h} - M_i)$$

2.3.5 Mercury intrusion porosimetry

Pore structure characterization was conducted using an Autopore IV 9500 Micromeritics mercury porosimeter. The Hg pressure range was 0.1-60,000 psi (0.0007–414 MPa). Both the total connected porosity and the pore size distribution in the 0.004–300 µm diameter range were obtained.

3. RESULTS AND DISCUSSION

3.1 Carbonation rate

The purpose of this study is to analyse the influence of the activator used and its concentration on the carbonation rate of alkali-activated SiMn slag mortars. The carbonation rate (V_{CO2}) is calculated using the classic model [44–47], which relates the carbonation depth (x) with the square root of time (equation 3).

Equation 3 $$x = V_{CO_2} \cdot \sqrt{t}$$

Figure 2 shows the carbonation depth in mortars in the accelerated carbonation test. Table 2 shows the values of the carbonation rate constants calculated by applying equation 3 to the results obtained in the carbonation rate tests. In Figure 2, the points correspond to the experimental data. The lines show to the theoretical kinetic model resulting from entering the values of the carbonation rate constants in equation 3. In the mortars prepared with NaOH, the carbonation rate decreases with increasing %Na_2O, which is in agreement with other authors' results [16]. On the other hand, with WG, it is observed that there are no significant differences between 4.0% and 4.5% Na_2O. Both concentrations have the lowest carbonation rate. Although unlike with NaOH, the carbonation rate is the highest in the highest WG concentration (5.0% Na_2O). When comparing the two activators, in general, it can be observed that the carbonation rate is higher in the case of NaOH. The results show that WG offers a greater resistance against the advance of carbonation. While in the case of NaOH, its resistance is lower and in turn this decreases with lower concentration.

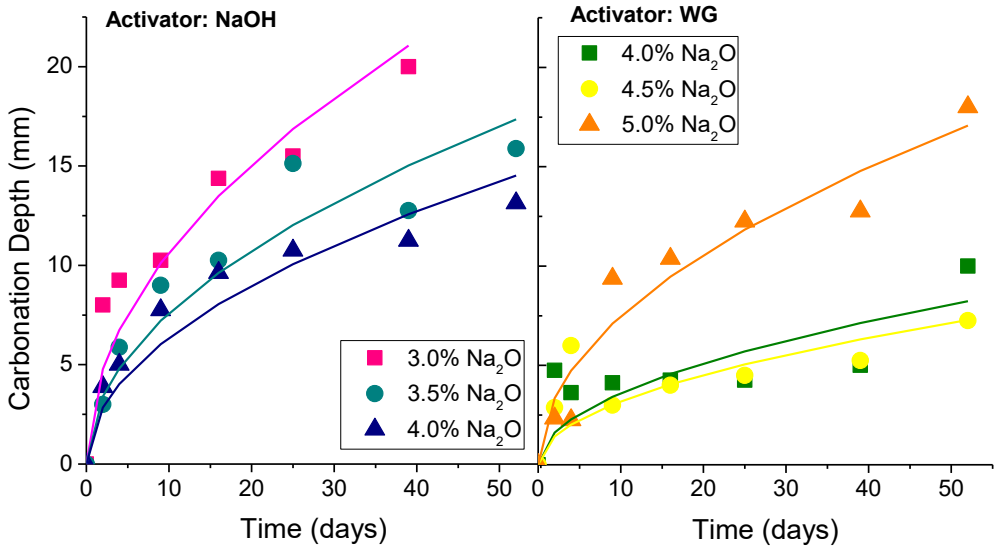

Figure 2. Carbonation depth evolution for mortars activated with NaOH (left) and WG (right) in a carbonation chamber (100% CO_2, 65 ± 5% RH).

Table 2. Carbonation rate (V_{CO2}) in mm/days$^{0.5}$ of the mortars in the accelerated carbonation test (100% CO_2, 65 ± 5% RH).

Activator	Concentration (% Na_2O)	V_{CO2} (mm/days$^{0.5}$)
NaOH	3.0	3.37
	3.5	2.41
	4.0	2.01
WG	4.0	1.14
	4.5	1.01
	5.0	2.37

This behaviour has been previously reported, where the mechanism of carbonation is strongly influenced by the type of precursor and the nature and concentration of the activator [18,48,49]. The mechanism of carbonation in alkali-activated slag is different from that which takes place in Portland cement. According to various authors [19,20,50], the carbonation of this material occurs directly in the C–A–S–H gel because of the lack of portlandite, leaving an alumina-containing remnant siliceous gel in addition to $CaCO_3$. However, the type of alkaline activator determines the composition and structure of the C-A-S-H gel formed. Puertas et al. [51] concluded that when WG was used the calcium silicate hydrate is characterised by long silicate chains and a low structural order with a low Ca/Si ratio. The calcium silicate hydrate formed in the pastes activated with NaOH has shorter chains, contains more Al in its structure and a higher Ca/Si ratio.

Mercury intrusion porosimetry results of two mortars activated with NaOH (4.0 %Na_2O) and WG (5.0 % Na_2O) before and after the carbonation process are presented in Table 3. It can be observed that the total porosity of the mortar activated with NaOH is greater than the one with WG. In both cases, this porosity increases after the carbonation process, especially in the case of NaOH. This fact agrees with the results reported by previous works [8,50], in which it is concluded that carbonation of alkali-activated materials lead to an increase in the total porosity. However, other authors distinguish a different behaviour for samples activated with NaOH, for which carbonation reduces the porosity, and those ones activated with WG, for which carbonation increases porosity [16,19]. Mercury retained is representative of how tortuous the network of pores is. The mortar activated with WG presents a more tortuous network of pores

than the one activated with NaOH. After carbonation, a reduction in this value occurs. This change due to the carbonation process would have its origin in the microstructural change produced by the chemical processes previously commented and it agrees with the increase of the porosity.

Table 3. Total porosity and Hg retained of two mortars activated with NaOH (4.0 %Na_2O) and WG (5.0 %Na_2O) before and after the carbonation process.

Activator	Concentration (% Na_2O)	Carbonation period (days)	Total porosity (%)	Hg Retained (%)
NaOH	4.0%	0	9.97	54.60
NaOH	4.0%	120	11.27	49.58
WG	5.0%	0	8.74	77.41
WG	5.0%	120	9.00	68.21

Figure 3 shows pore size distributions of the same mortars activated with NaOH (4.0 %Na_2O) and WG (5.0 %Na_2O) before and after the carbonation process. As it can be observed, most of the porosity volume of the mortar active with NaOH is located in pores with diameter less than 0.01 µm. In addition, the mortar activated with WG exhibits a more uniform distribution throughout the porosity range, although it has a slightly higher percentage of pores with a larger diameter compared to the previous activator. In this way, mortars prepared with NaOH showed higher porosity within the pore range of the technique used (from 0.0035 µm to 250 µm) than mortars activated with WG, which is in accordance to Shi in a previous study [4]. Therefore, the lower porosity of mortars activated with WG together with its greater tortuosity could be responsible for the lower carbonation rate and less depth due to the greater difficulty of entering CO_2.

On the other hand, after the carbonation process it is observed that in the case of NaOH there is a quite significant reduction of the pores with diameter <0.01 µm favouring the appearance of pores of greater size (0.01-0.1 µm). With WG, a decrease in pore range 100-10 µm and an increase in the range of smaller pores are observed (1-0.01 µm). These observation are opposite to what is reported by other authors [19], although the differences in the particular dosages, type of slag and curing times could produce a different behaviour.

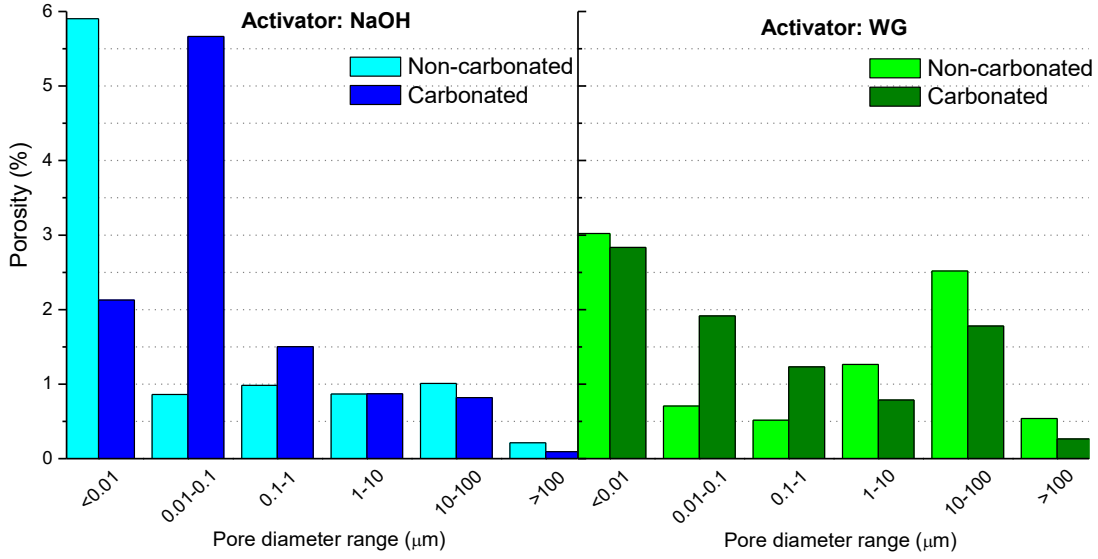

Figure 3. Pore size distributions of two mortars activated with NaOH (4.0 %Na_2O) and WG (5.0 %Na_2O) before and after the carbonation process.

Figure 4 shows the various crystalline phases compounding mortars activated with NaOH (4.0 %Na_2O) and WG (5.0 %Na_2O) before and after carbonation process. The peaks of greatest intensity seen in the diffractograms correspond to quartz (Q, ICDD: 00-005-0490) which is the main constituent of the aggregate in the mortar. Due to the intensity of this compound, no large differences are observed between the different diffractograms. In the mortar activated with NaOH the presence of calcite (C, ICDD: 00-005-0586), anorthoclase (A, ICDD: 00-010-0361), sodium aluminum silicate (S, ICDD: 01-080-1561) and gaylussite (G, ICDD: 00-002-0528) is observed. With the WG activator, the same compounds can be observed as with NaOH. As it has been previously commented, since there is not a phase able to be easily carbonated phase similar to portlandite in the case of cement-based binders, the carbonation proceeds by an attack to the C-A-S-H gel. This phase does not react in the same extent than portlandite so the formation of crystalline carbonation products is limited. Besides, the presence of such a high quantity of quartz hinders the detection of other minor crystalline phases. Additionally, it has not been detected the presence of layered double hydroxides (LDHs) as other authors have reported [22]. Also, due to the relatively low content of MgO in the SiMn slag (4.6%), detectable quantities of hydrotalcite-type phases (Mg-Al-LDH) are not expected in the XRD analysis. In the same way, phases with AFm structure (strätlingite-type Ca-Al-LDH) have not been observed, which is probably due to their low crystallinity that makes difficult their detection by XRD [52].

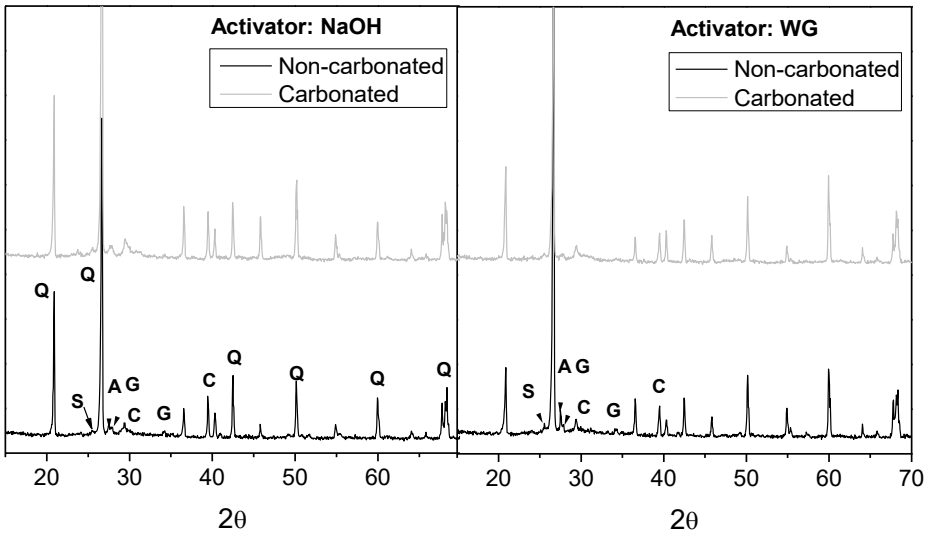

Figure 4. Mortar diffractograms before and after carbonation. C = Calcite, A = Anorthoclase, S = sodium aluminum silicate, G = gaylussite.

Next, the variation of the mechanical properties of the mortars studied due to the carbonation process is analysed. Figure 5 shows the data obtained for the flexural and compressive strengths of the mortars activated with NaOH and WG at different concentrations before and after the carbonation process.

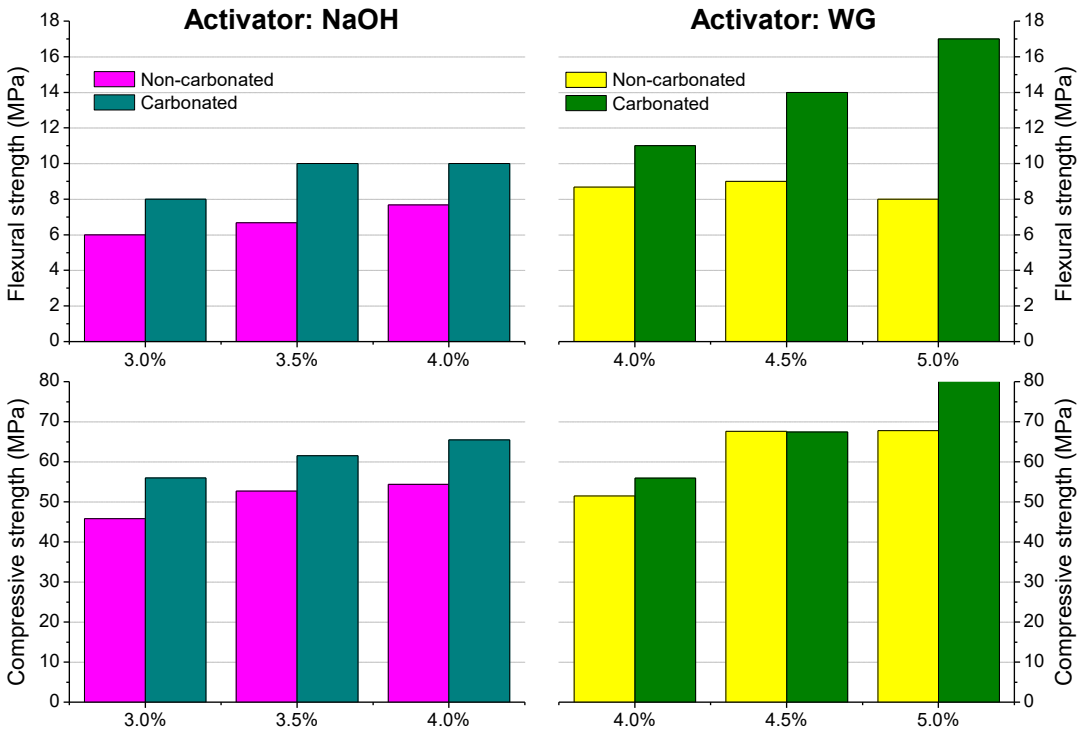

Figure 5. Flexural and compressive strengths of the mortars studied before and after the carbonation process.

The general trend is very clear. In all cases, regardless of the activator used, the carbonation produces an increase in the flexural and compressive strength of mortars. Other authors have reported opposite effect of the carbonation when using WG as activator [8,16,50]. If NaOH is used as activating solution, both trends have been reported, a decrease due to carbonation [8,50] or an increase [16,19]. The improvement that has been observed in present research is much more important in the case of NaOH, in which an increase in the compressive strength up to 22% has been registered. In the case of the WG, the improvement in compressive strength is not so remarkable. In this aspect, this activator shows a behaviour similar to Portland cement [44–47]. In the case of AAM, and according Bakharev et al. the carbonation process conducted decalcification of the C-A-S-H gel, but in this case, the carbonated mortar presents greater internal cohesion, possibly as a result of the precipitation of greater amounts of calcium carbonate in the pores, causing an increase in mechanical strength [20]. They explain that the increase of the CO_2 penetration rate, despite the low porosity, is due to the appearance of a large number of microscopic cracks associated with the shrinkage of the mortar during its previous curing process. Decalcification prompts a loss of cohesion in the mortar, which would explain the decline in mechanical strength. The extended curing period that has been implemented in present research, could avoid the appearance of microcracks in the mortars that would be developed in other AAM in which a shorter curing time is applied. Song et al. [53] also observed a decrease in the compressive strength of alkali-activated slag using WG as activator by carbonation, due to the fact that during the process the C-A-S-H of alkali-activated slag turned into amorphous silica gel. However, in the present study, the slight improvement of the mechanical properties can be attributed to the lower porosity of the mortar activated with WG that would offer an improved resistance to the carbonation penetration. In fact, it has been previously seen in Table 3 that the total porosity of the mortar practically does not change after the carbonation process in the case of using WG. Also during the process there has been a

reduction in pore diameter range which could explain the behaviour of this material despite the shrinkage suffered during curing [29].

Additionally, it should be noted that the chemistry of the SiMn slag is different to the materials activated in other works. The activation of slags with different chemical compositions would lead to the formation of different phases and the development of different microstructure. Then, a different behaviour could also be expected in the carbonation process.

Finally, it is worth noting that after the carbonation process, which consisted in very aggressive conditions (50 days in an almost 100% CO_2 atmosphere), the values of compressive strength are higher than 40 MPa. This mechanical performance could be considered high enough for a wide range of applications, which is consistent with the observations made by other authors [3,16,19].

3.2 Capillarity

Table 4 shows the capillary absorption coefficients (C_{90min} and C_{24h}) for mortars made with different activators and concentrations.

Table 4. Capillary absorption coefficients according to the concentration and type of activator.

Activator	% Na_2O	C_{90min} kg/m^2 min$^{0.5}$	C_{24h} kg/m^2 min$^{0.5}$
NaOH	3.0	0.417	11.73
	3.5	0.522	11.00
	4.0	0.546	10.59
WG	4.0	0.348	10.74
	4.5	0.274	9.59
	5.0	0.307	8.81

The mortars activated with NaOH show higher capillary absorption coefficients than those activated with WG. These results are consistent with the porosity previously observed (see Figure 3). In this way, NaOH has higher capillary suction velocity because its pore network is larger and also less tortuous. In both cases, a decrease in the capillary absorption coefficient C_{24h} is observed when increasing the concentration of the activator. This trend is also logical showing a denser matrix by increasing the concentration of activator, which supports the fact that the compressive strength increases (see Figure 5).

3.3 Chloride migration test

The results of chloride migration coefficient (D_{NTB}) obtained for the studied mortars are summarized in Table 5. WG activator produced mortars with higher migration coefficient than mortars prepared with NaOH. As it was previously commented, mortars fabricated with WG has a lower porosity, a more tortuous network of pores and a lower capillary suction velocity. From these characteristics the opposite tendency would be expected. Despite the lower total porosity exhibited by mortars prepared with WG, their pore size distributions show a higher volume of large pores. For instance, WG (5.0% Na_2O) presents values of 1.26% (1-10 µm), 2.52% (10-100 µm) and 0.54% (>100 µm) compared to NaOH (4.0% Na_2O) that has 0.87% (1-10 µm), 1.01% (10-100 µm) and 0.21% (>100 µm). Ionic diffusion and migration mechanisms are greatly supported by the porosity range of higher diameter, whereas capillary suction is mainly ruled by the narrower porosity [54]. This would be the reason of having these apparently opposite results. In terms of durability performance, both transport mechanism should be considered (capillarity and diffusion) and depending on the particular process or service conditions, the importance of the role played by them could be different. Additionally, a decrease in the migration coefficient is observed when increasing the concentration of activator used, which is consistent with the results of previous works [23]. This fact would be consistent with the denser matrix formed when

the %Na_2O is increased, which would be supported with the better mechanical performance of mortars with higher activator concentration.

Table 5. Results of non-steady-state chloride migration coefficient for the mortars studied.

Activator	% Na_2O	D_{NTB} x 10^{-12} (m^2/s)
NaOH	3.0	2.13±0.86
	3.5	1.27±0.29
	4.0	0.78±0.04
WG	4.0	5.62±0.57
	4.5	3.42±0.32
	5.0	2.62±0.08

The matrix obtained as a result of the alkali activation process of the slag would not offer a significant chloride binding capacity since, as it was previously shown by XRD analyses, it has been proved the absence of Mg-Al hydrotalcite-like products due to the low MgO content in the SiMn slag. The Mg/Al molar ratio of this slag is in the range of 0.5 to 0.6, which is much lower than the typical value presented by the hydrotalcite-like minerals, which is in the range of 2-3 [22]. This fact would lead to a lack of chloride binding capacity through the surface adsorption and inter-layer ion-exchange mechanisms in the Mg-Al hydrotalcite-like phases, as it has been established by other authors [21]. For this reason, the reduced chloride ingress of AAM, in comparison to OPC-based materials [23], which typically offer D_{NTB} values around 10^{-11} m^2/s, would arise from a better pore structure, i.e. finer porosity and higher tortuosity.

3.4 Corrosion tests

Usually, reinforced concrete rebars are passivated due to the high pH level provided by the cement hydration products. Nevertheless, some circumstances can destroy passive film on the steel surface. In Portland cement-based materials, the main processes leading to the destruction of the passive film are the carbonation of concrete cover and/or the presence of chlorides over the critical concentration threshold. Then, the transition from passive to active state occurs, and as a consequence, the structural element service life rapidly decreases. However, in AAMs, the situation is more complex due to the presence of sulphides in the slag, which may hinder the formation of the passive layer on the steel surface [23,25].

As it has been observed in other works [26], the corrosion rate ranges that have been applied to analyse the results are based on the same criteria that usually applied to Portland cement-based systems, which were introduced by Andrade and Alonso [55]. These criteria establish the following levels for the corrosion rate of the steels: below 0.1 $\mu A/cm^2$ indicates a passive state of the steel; the 0.1-0.5 $\mu A/cm^2$ range corresponds to low corrosion rate; 0.5-1.0 $\mu A/cm^2$ range show high level of corrosion; and above 1.0 $\mu A/cm^2$ indicates very high corrosion rate. These criteria can only be applied in cases where the corrosion process affects all the steel surface (generalized corrosion) but not to those cases where pitting corrosion takes place (localised corrosion).

Figure 6 shows the evolution of corrosion rate and corrosion potential of the steel bars embedded in SiMn slag mortars activated with NaOH and WG during an accelerated carbonation process. All the graphs are divided into three zones: the first one corresponds to the curing time in a humid chamber with 100% relative humidity, the second corresponds to the stabilization time under laboratory conditions (20 ± 2°C and 50% RH) and the third zone corresponds to the accelerated carbonation process. At the beginning of the process, corrosion rate values of the steel are high since the passivation process implies the formation of a thin protective film of iron oxides, which are generated by the oxidation (corrosion) of the steel surface. Then values progressively decrease towards non active corrosion values for all mortars. However, the

passivation process takes more time in mortars activated with NaOH than with WG. The reason for this difference could be due to a lower availability of oxygen at the steel-mortar interface, as it was suggested by other authors [56,57]. Steel embedded in control mortars that have been kept in laboratory conditions have shown Ecorr values around -0.1 V and low Icorr values for both types of activators. This would indicate the existence of stable passive films, and is in agreement with the results shown by other authors in studies concerning granulated blast furnace slag and its combination with SiMn slag [26].

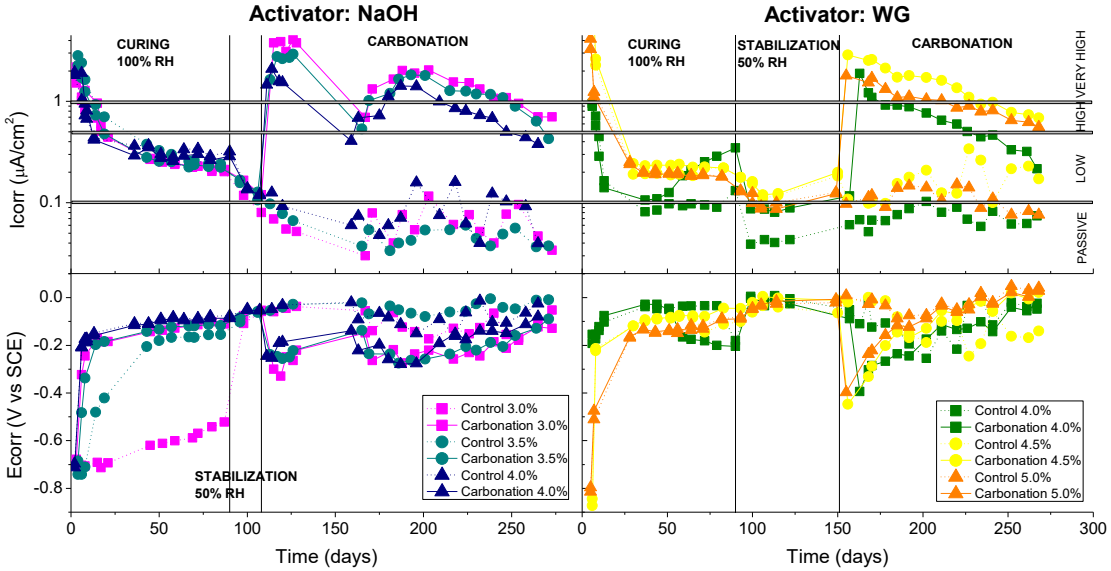

Figure 6. Corrosion rate and corrosion potential of steel embedded in mortars activated with NaOH (left) and WG (right) in accelerated carbonation environment (100% CO_2 and 65±5% RH).

For both activators, in just ten days the carbonation front reaches the steel surface and corrosion rates increases. With NaOH, and as it was previously observed in the study of carbonation kinetics, the carbonation rate increases as the percentage of Na_2O decreases. With the activator WG, the mortar with 4.0% Na_2O concentration shows the lowest corrosion rate, although between 4.5 and 5.0% Na_2O the behavior is similar. Taking into account the previous carbonation rate study, the two activators should show slightly different behaviors. In the case of the NaOH activator, it was found that the carbonation rate is higher than with WG, whereas it is clear here that both activators show similar Icorr values. The possible reason for this behavior could be due to the fact that the mortars activated with WG, despite having a lower porosity and greater tortuosity, suffer greater shrinkage in the experimental conditions of the test [29], which causes microcracking and therefore, CO_2 can quickly reach the steel reinforcement surface and initiate corrosion. Other authors also observed this greater shrinkage when WG was used as activator [19]. Besides, the carbonation rate would affect the length of the corrosion initiation time, i.e. the time from the beginning of the attack to the activation of the corrosion process. The corrosion rate that is reached after the initiation stage, is also affected but other parameters such as the oxygen diffusion rate, which is in turn mainly affected by the transport properties of the mortar cover, the relative humidity and the temperature. As the microcracking is expected to start in the pre-conditioning stage (50% RH), but it would develop in the following weeks, its influence would be greater at longer ages, i.e. in the corrosion propagation period. That hypothesis could explain the slight differences observed between the carbonation rate and the corrosion rate with both types of activators. Therefore, apparently the nature of the activator has practically no influence on this property since both mortars exhibit a very similar behavior and both types of activators cannot be considered to provide a more protective chemical environment against the steel corrosion in a carbonation process.

Figure 7 shows the evolution of corrosion rate and corrosion potential of the steel bars embedded in mortars activated with NaOH and WG, whose specimens have been partially submerged in seawater.

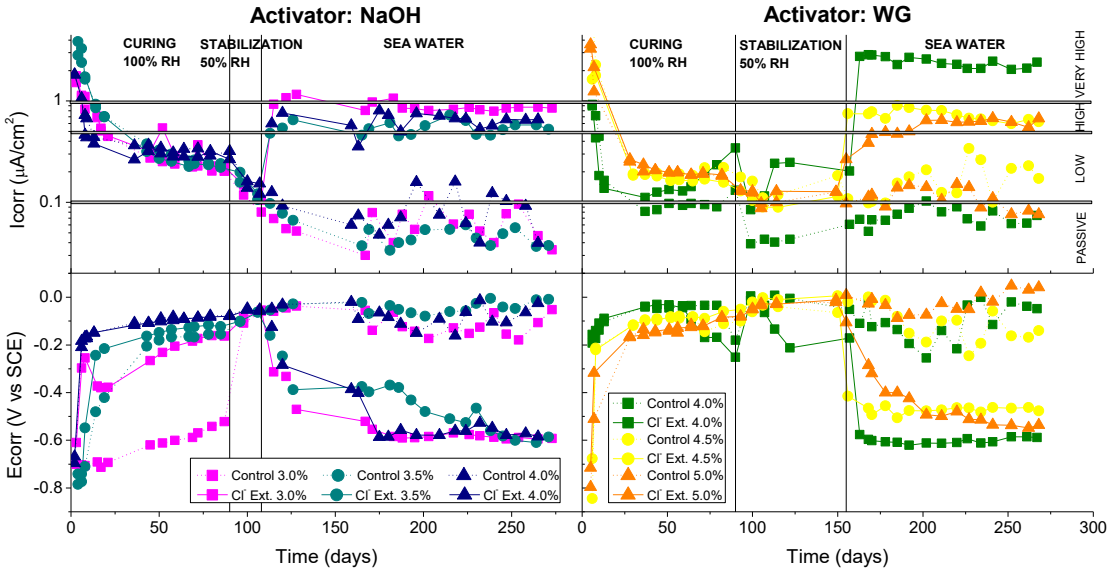

Figure 7. Corrosion rate and corrosion potential of steel embedded in mortars activated with NaOH (left) and WG (right), partially immersed in sea water.

The behavior during the initial passivation is similar to the previously commented in the carbonation tests. The formation of the passivation film was quicker in the case of using WG as activator. In the same way, in about ten days both activators reach appreciable corrosion rates. It can be seen that in the case of NaOH, the three activator concentrations studied show very similar Icorr values. Mortars activated with WG also show a similar behavior in the concentrations 4.5% and 5.0% Na_2O, reaching values similar to those seen with the other activator. The only mortar that differs from the general behavior is the one with 4.0% Na_2O and WG. In this case, it shows greater corrosion, as can be seen in Figure 7. A short corrosion initiation period could be related with a high chloride diffusion coefficient [21], and it can be observed that this particular mortar registered the higher chloride diffusion coefficient of this work. The shrinkage suffered by the mortar could be responsible for this greater corrosion. In a previous study [29], the shrinkage experienced by mortars activated with NaOH and WG was studied. In that work, it was reported that the mortar with WG and 4.0% Na_2O suffered the greatest shrinkage. These short initiation times of the corrosion process are also in agreement with the negligible chloride binding capacity of the binders that was previously commented.

Figure 8 shows the evolution of Icorr and Ecorr of the steels embedded in mortars activated with different concentrations of NaOH in which different percentages of chlorides have been added (0.0 (Control), 0.5, 1.0, 2.0 and 4.0% wt respect to slag mass).

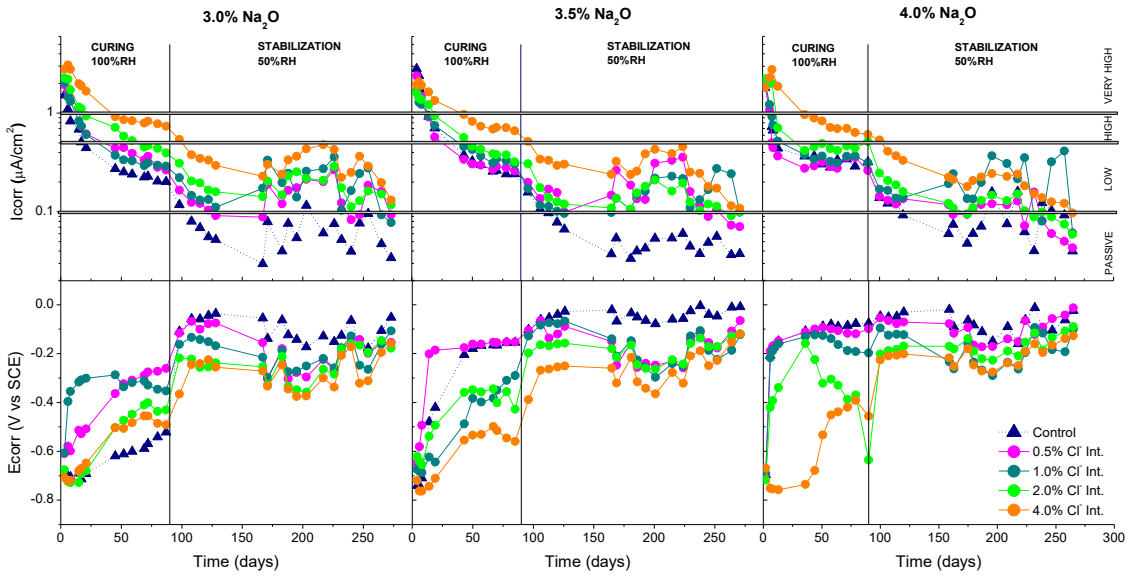

Figure 8. Corrosion rate and corrosion potential of steel embedded in mortars activated with NaOH at three different concentrations (left: 3.0% Na_2O; centre: 3.5% Na_2O; right: 4.0% Na_2O), for different percentages of addition of chlorides with respect to the slag mass.

Initially it is observed that there are high values of corrosion due to the passivation process of the steels. These levels are gradually falling to stable values. In the part of Figure 8 corresponding to the corrosion potential, a clear ordering of the values can be observed as a function of the amount of chlorides added in the mix. The higher this percentage is, the more negative is the potential for corrosion. This trend is the expected one, since a lower corrosion potential indicates more tendency towards corrosion. In the upper part of Figure 8 some ordering of the values is also observed. In general, the higher chloride content, the higher values of Icorr of the steel in the mortars. Control mortars are stably below the active corrosion threshold (0.1 $\mu A/cm^2$). At low concentrations of activator (3.0% and 3.5% Na_2O), when adding the different chloride concentrations, the curves fluctuate between the active zone and the threshold zone (low zone). In contrast, in the highest concentration of activator (4.0% Na_2O), Icorr curves decrease more and only high concentrations of chloride are located in the active zone (low zone).

Figure 9 shows the evolution of Icorr and Ecorr of the steel embedded corresponding to mortars activated with different concentrations of WG. The general tendencies of the Icorr and Ecorr values are similar to those observed with NaOH as activator. However, a greater difference can be seen between the control mortars and the mortars with internal chlorides. The curves of Icorr are clearly located in the active area of corrosion even at low concentrations of chlorides.

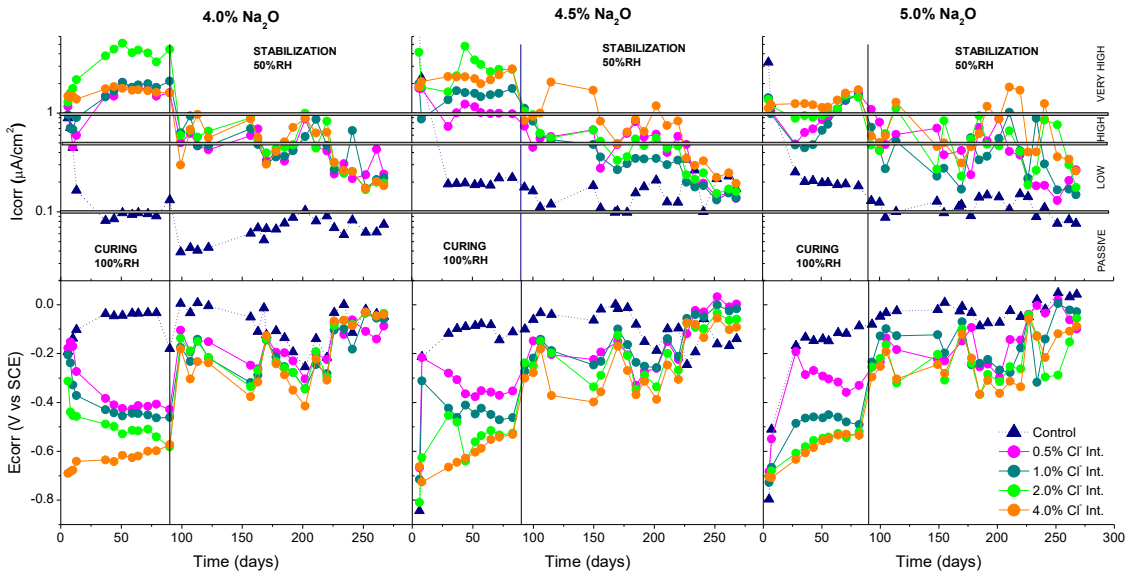

Figure 9. Corrosion rate and corrosion potential of steel embedded in mortars activated with WG at three different concentrations (left: 4.0% Na_2O; centre: 4.5% Na_2O; right: 5.0% Na_2O), for different percentages of addition of chlorides with respect to the slag mass.

Figure 10 shows the average value of the corrosion rate and corrosion potential corresponding to the final section where the values tend to stabilize for both mortars activated with NaOH and those activated with WG.

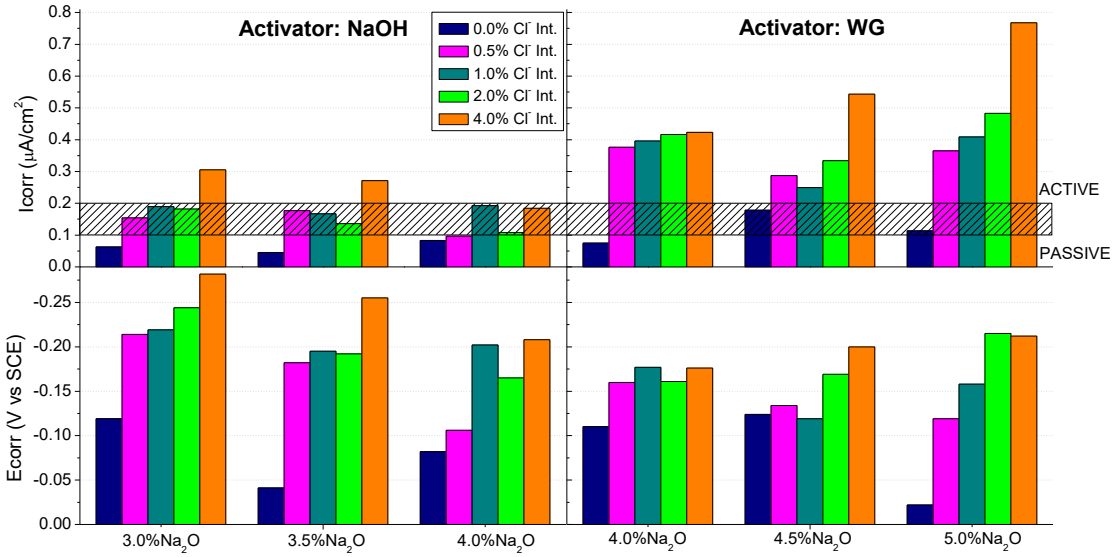

Figure 10. The average value of the corrosion rate and corrosion potential of steel embedded in mortars activated with NaOH (left) and WG (right), for different percentages of addition of chlorides with respect to the slag mass.

In Figure 10 the tendency of the Icorr and Ecorr values for each one of the activators can be observed more clearly. The Ecorr value of the steels of the mortars activated with NaOH with 0% chlorides logically shows the least negative value. In the case of the concentrations of 3.0% and 3.5% of Na_2O, it can be seen that by adding 0.5% chloride, the registered corrosion potential decreases significantly. The value of Ecorr continues to decrease as the concentration of chlorides in the mortar increases, reaching its highest negative value with 4.0% chloride with respect to the slag mass. However, in the mortar with the highest concentration of activator

(4.0% Na_2O), it can be observed that the greatest change in the Ecorr value occurs when adding 1.0% chloride. If the tendency of the Icorr values is then observed, it can be seen that as the concentration of internal chlorides increases, its value increases. However, all steels corresponding to mortars with 0, 0.5, 1.0 and 2.0% chloride concentrations are stably below the active corrosion threshold (0.1 $\mu A/cm^2$). In the case of concentrations of 3.0 and 3.5% Na_2O activator, only the steels of the mortars with 4.0% of chlorides, despite the differences in the values of Ecorr, are located in the active zone. This may be indicative that the chloride threshold for this type of mortar may be situated between 2.0% and 4.0% chloride with respect to the slag mass. In the highest concentration of activator (4.0% Na_2O) all the values are below the active zone. This may indicate that steels embedded in those mortars may even withstand that amount of chlorides for some time. This behaviour was also previously reported by Babaee et al., who attributed the higher chloride threshold of binders with higher activator concentration to the development of a more homogenous binder and, as a result, a less permeable passive layer on the steel surface [21]. Nevertheless, it should be noted that the saw-shaped evolution of the Icorr values is typically associated to the competing effect between hydroxyl and chloride ions which precedes the corrosion pit formation [58].

In the case of steels embedded in the binder activated with WG, it is clearly observed that the corrosion rate values are higher and only control mortar correctly protects the steel. Any chloride concentration higher than 0.5% respect to slag mass induces an active corrosion process. For this reason, the chloride threshold for this binder may be located below 0.5% respect to binder mass. In other studies it is concluded that slag rich systems could develop passive films with a reduced stability because the oxidation of sulphide ions hinders the oxidation of iron and, therefore, the proper formation of the passive layer [21]. Additionally, according to previous works, the explanation for this behaviour may be found in a mechanism by which not only the amount of chlorides that reaches the steel surface has to be considered in a chloride-induced corrosion process, but also the hydroxyl ions concentrations [58]. In that study, it is stated that there is a competing process between the passivating action of hydroxyls and the pitting formation of chlorides, and conclude that the $[Cl^-]/[OH^-]$ ratio should be used to establish the threshold from which the corrosion is active. When Portland cement is used as a binder, the hydroxyl concentration is almost constant since it is controlled by the buffer action of portlandite, so it is licit to only consider the chloride concentration as the trigger to activate the corrosion. However, in present case, a different hydroxyl concentration is expected, which arise from: the absence of portlandite and the different chemistry of the activating solution. If NaOH is used as activator, a higher hydroxyl concentration is expected, which is also supported by the commented difficulties to get a stable passivating film. That would lead that mortar to withstand a higher chloride concentration in comparison to the lower chloride concentration that is needed in the mortar with WG to initiate the chloride-induced corrosion process.

4. CONCLUSIONS

The following conclusions can be drawn from the results obtained in this study:

1. The results show that WG offers a greater resistance against the advance of carbonation. While in the case of NaOH, its resistance is lower and it decreases with lower concentration.
2. In all cases, regardless of the activator used and its concentration, the carbonation produces an increase in the flexural and compressive strength of mortars.
3. Mortars activated with NaOH showed higher capillary absorption coefficients than those activated with WG. A decrease in the capillary absorption coefficient C_{24h} is observed when increasing the concentration of the activator.
4. WG activator produced mortars with higher chloride migration coefficient than mortars prepared with NaOH. Additionally, a decrease in the chloride migration coefficient is observed when increasing the concentration of activator used.

5. The nature of the activator has practically no influence on carbonation-induced corrosion of steels since both mortars exhibited a very similar behavior and both types of activators cannot be considered to provide a more protective chemical environment against the steel corrosion in a carbonation process.
6. Steels embedded in mortars prepared with NaOH offered lower corrosion rate levels in a chloride-contaminated ambient, and corrosion rate increased with the activator concentration independently of the type of activator.

ACKNOWLEDGEMENT

The authors wish to thank the Spanish Ministry of Economy and Competitiveness and European Union (FEDER) for project funding (BIA 2014-58194-R). The authors also wish to thank Cristina Rodríguez from Ferroatlántica, S.A., for the supply of SiMn slag necessary to carry out this research.

REFERENCES

[1] A. Palomo, P. Krivenko, I. Garcia-Lodeiro, E. Kavalerova, O. Maltseva, A. Fernández-Jiménez, A review on alkaline activation: new analytical perspectives, Mater. Construcción. 64 (2014) e022. doi:10.3989/mc.2014.00314.

[2] J.L. Provis, Geopolymers and other alkali activated materials: Why, how, and what?, Mater. Struct. Constr. 47 (2014) 11–25. doi:10.1617/s11527-013-0211-5.

[3] E. Rodríguez, S. Bernal, R. Mejía de Gutiérrez, F. Puertas, Alternative concrete based on alkali-activated slag, Mater. Constr. 58 (2008) 53–67. doi:org/10.3989/mc.2008.v58.i291.104.

[4] C. Shi, Strength, pore structure and permeability of alkali-activated slag mortars, Cem. Concr. Res. 26 (1996) 1789–1799. doi:10.1016/S0008-8846(96)00174-3.

[5] H. Zhu, Z. Zhang, Y. Zhu, L. Tian, Durability of alkali-activated fly ash concrete: Chloride penetration in pastes and mortars, Constr. Build. Mater. 65 (2014) 51–59. doi:10.1016/j.conbuildmat.2014.04.110.

[6] A. Mobili, A. Belli, C. Giosuè, T. Bellezze, F. Tittarelli, Metakaolin and fly ash alkali-activated mortars compared with cementitious mortars at the same strength class, Cem. Concr. Res. 88 (2016) 198–210. doi:10.1016/j.cemconres.2016.07.004.

[7] J.L. Provis, Alkali-activated materials, Cem. Concr. Res. (2016). doi:10.1016/j.cemconres.2017.02.009.

[8] S.A. Bernal, J.L. Provis, Durability of alkali-activated materials: Progress and perspectives, J. Am. Ceram. Soc. 97 (2014) 997–1008. doi:10.1111/jace.12831.

[9] P. Duxson, J.L. Provis, G.C. Lukey, J.S.J. van Deventer, The role of inorganic polymer technology in the development of “green concrete,” Cem. Concr. Res. 37 (2007) 1590–1597. doi:10.1016/j.cemconres.2007.08.018.

[10] A. Mellado, C. Catalán, N. Bouzón, M. V Borrachero, J.M. Monzó, J. Payá, Carbon footprint of geopolymeric mortar: Study of the contribution of the alkaline activating solution and assessment of an alternative route, RSC Adv. 4 (2014) 23846–23852. doi:10.1039/c4ra03375b.

[11] L.K. Turner, F.G. Collins, Carbon dioxide equivalent (CO2-e) emissions: A comparison between geopolymer and OPC cement concrete, Constr. Build. Mater. 43 (2013) 125–130. doi:10.1016/j.conbuildmat.2013.01.023.

[12] B.C. McLellan, R.P. Williams, J. Lay, A. Van Riessen, G.D. Corder, Costs and carbon emissions for geopolymer pastes in comparison to ordinary portland cement, J. Clean. Prod. 19 (2011) 1080–1090. doi:10.1016/j.jclepro.2011.02.010.

[13] J. Zhang, C. Shi, Z. Zhang, Z. Ou, Durability of alkali-activated materials in aggressive environments: A review on recent studies, Constr. Build. Mater. 152 (2017) 598–613. doi:10.1016/j.conbuildmat.2017.07.027.

[14] M. Pourbaix, Some applications of potencial-pH diagrams to study of localized corrosion,

682 J. Electrochem. Soc. 123 (1976) C25–C36. doi:10.1149/1.2132800.
683 [15] I. Ismail, S.A. Bernal, J.L. Provis, R. San Nicolas, D.G. Brice, A.R. Kilcullen, S. Hamdan, J.S.J.
684 Van Deventer, Influence of fly ash on the water and chloride permeability of alkali-
685 activated slag mortars and concretes, Constr. Build. Mater. 48 (2013) 1187–1201.
686 doi:10.1016/j.conbuildmat.2013.07.106.
687 [16] Z. Shi, C. Shi, S. Wan, N. Li, Z. Zhang, Effect of alkali dosage and silicate modulus on
688 carbonation of alkali-activated slag mortars, Cem. Concr. Res. 113 (2018) 55–64.
689 doi:10.1016/j.cemconres.2018.07.005.
690 [17] S.A. Bernal, R. San Nicolas, R.J. Myers, R. Mejía de Gutiérrez, F. Puertas, J.S.J. van
691 Deventer, J.L. Provis, MgO content of slag controls phase evolution and structural
692 changes induced by accelerated carbonation in alkali-activated binders, Cem. Concr. Res.
693 57 (2014) 33–43. doi:10.1016/j.cemconres.2013.12.003.
694 [18] S.A. Bernal, R. San Nicolas, J.L. Provis, R. Mejía De Gutiérrez, J.S.J. Van Deventer, Natural
695 carbonation of aged alkali-activated slag concretes, Mater. Struct. Constr. 47 (2014) 693–
696 707. doi:10.1617/s11527-013-0089-2.
697 [19] F. Puertas, M. Palacios, T. Vázquez, Carbonation process of alkali-activated slag mortars,
698 J. Mater. Sci. 41 (2006) 3071–3082. doi:10.1007/s10853-005-1821-2.
699 [20] T. Bakharev, J.G. Sanjayan, Y.B. Cheng, Resistance of alkali-activated slag concrete to
700 carbonation, Cem. Concr. Res. 31 (2001) 1277–1283. doi:10.1016/S0008-8846(01)00574-
701 9.
702 [21] M. Babaee, A. Castel, Chloride diffusivity, chloride threshold, and corrosion initiation in
703 reinforced alkali-activated mortars: Role of calcium, alkali, and silicate content, Cem.
704 Concr. Res. 111 (2018) 56–71. doi:10.1016/j.cemconres.2018.06.009.
705 [22] X. Ke, S.A. Bernal, J.L. Provis, Uptake of chloride and carbonate by Mg-Al and Ca-Al
706 layered double hydroxides in simulated pore solutions of alkali-activated slag cement,
707 Cem. Concr. Res. 100 (2017) 1–13. doi:10.1016/j.cemconres.2017.05.015.
708 [23] Q. Ma, S. V. Nanukuttan, P.A.M. Basheer, Y. Bai, C. Yang, Chloride transport and the
709 resulting corrosion of steel bars in alkali activated slag concretes, Mater. Struct. 49 (2016)
710 3663–3677. doi:10.1617/s11527-015-0747-7.
711 [24] J. Shi, J. Ming, W. Sun, Electrochemical behaviour of a novel alloy steel in alkali-activated
712 slag mortars, Cem. Concr. Compos. 92 (2018) 110–124.
713 doi:10.1016/j.cemconcomp.2018.06.004.
714 [25] W. Aperador, R. Mejía de Gutiérrez, D.M. Bastidas, Steel corrosion behaviour in
715 carbonated alkali-activated slag concrete, Corros. Sci. 51 (2009) 2027–2033.
716 doi:10.1016/j.corsci.2009.05.033.
717 [26] M. Criado, S.A. Bernal, P. Garcia-Triñanes, J.L. Provis, Influence of slag composition on
718 the stability of steel in alkali-activated cementitious materials, J. Mater. Sci. 53 (2018)
719 5016–5035. doi:10.1007/s10853-017-1919-3.
720 [27] R. Navarro, E. Zornoza, P. Garcés, I. Sánchez, E.G. Alcocel, Optimization of the alkali
721 activation conditions of ground granulated SiMn slag, Constr. Build. Mater. 150 (2017)
722 781–791. doi:10.1016/j.conbuildmat.2017.06.064.
723 [28] S. Kumar, P. García-Triñanes, A. Teixeira-Pinto, M. Bao, Development of alkali activated
724 cement from mechanically activated silico-manganese (SiMn) slag, Cem. Concr. Compos.
725 40 (2013) 7–13. doi:10.1016/j.cemconcomp.2013.03.026.
726 [29] R. Navarro, E.G. Alcocel, I. Sánchez, P. Garcés, E. Zornoza, Mechanical properties of alkali
727 activated ground SiMn slag mortars with different types of aggregates, Constr. Build.
728 Mater. 186 (2018) 79–89. doi:10.1016/j.conbuildmat.2018.07.093.
729 [30] J. Péra, J. Ambroise, M. Chabannet, Properties of blast-furnace slags containing high
730 amounts of manganese, Cem. Concr. Res. 29 (1999) 171–177. doi:10.1016/S0008-
731 8846(98)00096-9.
732 [31] F. Puertas, Escorias de alto horno: composición y comportamiento hidráulico, Mater.
733 Construcción. 43 (1993) 37–48. doi:10.3989/mc.1993.v43.i229.687.

[32] S.-D.D. Wang, K.L. Scrivener, P.L.L. Pratt, Factors affecting the strength of alkali-activated slag, Cem. Concr. Res. 24 (1994) 1033–1043. doi:10.1016/0008-8846(94)90026-4.
[33] A.G. De La Torre, S. Bruque, M.A.G. Aranda, Rietveld quantitative amorphous content analysis, J. Appl. Crystallogr. 34 (2001) 196–202. doi:10.1107/S0021889801002485.
[34] UNE 80225:2012. Methods of testing cement. Chemical analysis. Determination of reactive SiO2 content in cements, puzzolanas and fly ash, (2012).
[35] UNE 196-2:2014. Method of testing cement. Part 2: Chemical analysis of cement, (2014).
[36] UNE EN 196-6:2010. Methods of testing cement. Part 6: Determination of fineness, (2010).
[37] UNE 146301:2002. Aggregates. Fineness modulus of the fine aggregate, (2002).
[38] UNE-EN 1097-6:2014. Tests for mechanical and physical properties of aggregates. Part 6: Determination of particle density and water absorption, (2014).
[39] EN 196-1:2005. Methods of testing cement. Part 1: determination of strength, (2005).
[40] UNE 112011:1994. Corrosión en armaduras. Determinación de la profundidad de carbonatación en hormigones endurecidos y puestos en servicio, (1994).
[41] M. Stern, A.L. Geary, Electrochemical polarization 1. A theoretical analysis of the shape of polarization curves, J. Electrochem. Soc. 104 (1957) 56–63. doi:10.1149/1.2428496.
[42] NT Build 492, Concrete, mortar and cement-based repair materials: Chloride migration coefficient from non-steady-state migration experiments, Nord. Method. (1999) 1–8. doi:UDC 691.32/691.53/691.54.
[43] UNE-EN 1015-18:2003. Methods of test for mortar for masonry. Part 18: Determination of water absorption coefficient due to capillary action of hardened mortar, (2003).
[44] J. Khunthongkeaw, S. Tangtermsirikul, T. Leelawat, A study on carbonation depth prediction for fly ash concrete, Constr. Build. Mater. 20 (2006) 744–753. doi:10.1016/j.conbuildmat.2005.01.052.
[45] P. Sulapha, S.F. Wong, T.H. Wee, S. Swaddiwudhipong, Carbonation of Concrete Containing Mineral Admixtures, J. Mater. Civ. Eng. 15 (2003) 134–143. doi:10.1061/(ASCE)0899-1561(2003)15:2(134).
[46] T.H. Wee, A.K. Suryavanshi, D. Logendran, Pore structure controlling the carbonation of a hardened cement matrix blended with mineral admixture, Adv. Cem. Res. 11 (1999) 81–95. doi:10.1680/adcr.1999.11.2.81.
[47] P. Castro, M.A. Sanjuán, J. Genescá, Carbonation of concretes in the Mexican Gulf, Build. Environ. 35 (2000) 145–149. doi:10.1016/S0360-1323(99)00009-8.
[48] S.A. Bernal, J.L. Provis, B. Walkley, R. San Nicolas, J.D. Gehman, D.G. Brice, A.R. Kilcullen, P. Duxson, J.S.J. Van Deventer, Gel nanostructure in alkali-activated binders based on slag and fly ash, and effects of accelerated carbonation, Cem. Concr. Res. 53 (2013) 127–144. doi:10.1016/j.cemconres.2013.06.007.
[49] M. Palacios, F. Puertas, Effect of Carbonation on Alkali-Activated Slag Paste, J. Am. Ceram. Soc. 89 (2006) 3211–3221. doi:10.1111/j.1551-2916.2006.01214.x.
[50] J.L. Provis, A. Palomo, C. Shi, Advances in understanding alkali-activated materials, Cem. Concr. Res. 78 (2015) 110–125. doi:10.1016/j.cemconres.2015.04.013.
[51] F. Puertas, A. Fernández-Jiménez, M.. Blanco-Varela, Pore solution in alkali-activated slag cement pastes. Relation to the composition and structure of calcium silicate hydrate, Cem. Concr. Res. 34 (2004) 139–148. doi:10.1016/S0008-8846(03)00254-0.
[52] R.J. Myers, B. Lothenbach, S.A. Bernal, J.L. Provis, Thermodynamic modelling of alkali-activated slag cements, Appl. Geochemistry. 61 (2015) 233–247. doi:10.1016/j.apgeochem.2015.06.006.
[53] K. Il Song, J.K. Song, B.Y. Lee, K.H. Yang, Carbonation characteristics of alkali-activated blast-furnace slag mortar, Adv. Mater. Sci. Eng. 2014 (2014) 1–11. doi:10.1155/2014/326458.
[54] M. Shafikhani, S.E. Chidiac, Quantification of concrete chloride diffusion coefficient – A critical review, Cem. Concr. Compos. 99 (2019) 225–250.

doi:10.1016/j.cemconcomp.2019.03.011.
[55] C. Andrade, C. Alonso, Corrosion rate monitoring in the laboratory and on-site, Constr. Build. Mater. 10 (1996) 315–328. doi:10.1016/0950-0618(95)00044-5.
[56] S. Mundra, S.A. Bernal, M. Criado, P. Hlaváček, G. Ebell, S. Reinemann, G.J.G. Gluth, J. Provis, Steel corrosion in reinforced alkali-activated materials, RILEM Tech. Lett. 2 (2017) 33–39. doi:10.21809/rilemtechlett.2017.39.
[57] P. Hlaváček, S. Reinemann, G.J.G. Gluth, M. Rünger, G. Ebell, J. Mietz, H. -C. Kühne, Durability-related properties of geopolymer mortars, in: 6th Int. Conf. Non-Traditional Cem. Concr. Brno, Czech Repub., 2017.
[58] P. Garcés, A. Sáez, C.G. Andreu, C. Andrade, The Influence of the ratio [Cl-]/[OH-] on the corrosion rate of reinforcing steel in neutral and acid solutions, in: Mater. Sci. Forum,192-194, 1995: pp. 907–914.